Cerebral Cortex August 2013;23:1798–1810
doi:10.1093/cercor/bhs154
Advance Access publication June 17, 2012

Age-Based Comparison of Human Dendritic Spine Structure Using Complete Three-Dimensional Reconstructions

Ruth Benavides-Piccione[1,2,4], Isabel Fernaud-Espinosa[2], Victor Robles[3], Rafael Yuste[5] and Javier DeFelipe[1,2,4]

[1]Instituto Cajal (CSIC), 28002 Madrid, Spain [2]Laboratorio Cajal de Circuitos Corticales (CTB), [3]Departamento de Arquitectura y Tecnología de Sistemas Informáticos, Universidad Politécnica de Madrid (UPM), 28223 Madrid, Spain, [4]Centro de Investigación Biomédica en Red sobre Enfermedades Neurodegenerativas (CIBERNED), Spain and [5]Department of Biological Sciences, Columbia University, New York, NY 10027, USA

Address correspondence to Ruth Benavides-Piccione. Email: rbp@cajal.csic.es

Dendritic spines of pyramidal neurons are targets of most excitatory synapses in the cerebral cortex. Recent evidence suggests that the morphology of the dendritic spine could determine its synaptic strength and learning rules. However, unfortunately, there are scant data available regarding the detailed morphology of these structures for the human cerebral cortex. In the present study, we analyzed over 8900 individual dendritic spines that were completely 3D reconstructed along the length of apical and basal dendrites of layer III pyramidal neurons in the cingulate cortex of 2 male humans (aged 40 and 85 years old), using intracellular injections of Lucifer Yellow in fixed tissue. We assembled a large, quantitative database, which revealed a major reduction in spine densities in the aged case. Specifically, small and short spines of basal dendrites and long spines of apical dendrites were lost, regardless of the distance from the soma. Given the age difference between the cases, our results suggest selective alterations in spines with aging in humans and indicate that the spine volume and length are regulated by different biological mechanisms.

Keywords: cerebral cortex, confocal, intracellular, Lucifer Yellow, 3D reconstructions

Introduction

Dendritic spines of pyramidal neurons are thin protrusions emerging from dendrites, which are the sites of most excitatory synapses in the cerebral cortex. They are considered key elements in learning, memory, and cognition (Yuste 2010). Furthermore, all or almost all dendritic spines establish at least one excitatory glutamatergic synapse (Arellano, Espinosa et al. 2007), and therefore, changes in the number of spines in the dendritic arbors of neurons may influence both cellular and system cortical functions. Indeed, both the number and the density of dendritic spines located in different cortical areas and species present variations that may reflect functional differences characteristic of each cortical area. For example, a 2-fold difference in density have been reported within the mouse neocortex, whereas among cortical areas of primates, including humans, this difference can be up to 10-fold (Jacobs et al. 2001; Jacobs and Scheibel 2002; Elston et al. 2001; Elston 2007; Ballesteros-Yáñez et al. 2010; Elston et al. 2011). In addition, a correlation between morphological and functional parameters of spines has been reported. Specifically, the spine head volume is correlated with the area of the post-synaptic density, the number of post-synaptic receptors, and the ready-releasable pool of transmitter (Harris and Stevens 1989; Nusser et al. 1998; Schikorski and Stevens 1999, 2001; Arellano, Benavides-Piccione et al. 2007), whereas the length of the spine neck is proportional to the degree of biochemical and electrical isolation of the spine from its parent dendrite (Majewska, Brown et al. 2000; Majewska, Tashiro et al. 2000; Araya et al. 2006). Also, it has been shown that larger spines can generate greater synaptic currents than smaller spines (Matsuzaki et al. 2004). Furthermore, dendritic spines are dynamic structures with fluctuations in volume that seem to have important implications for cognition and memory (Dunaevsky et al. 1999; Matus 2000; Bonhoeffer and Yuste 2002; Kasai et al. 2010). Thus, the study of dendritic spine morphology is critical from the functional point of view.

Previous studies in primates, including humans, have shown that dendritic spines are sensitive to age, showing changes in spine density during development and lifespan (Rakic et al. 1994; Jacobs et al. 1997; Hof and Morrison 2004; Petanjek et al. 2008; Anderson et al. 2009; Kabaso et al. 2009; Dumitriu et al. 2010; Petanjek et al. 2011). However, there are no studies regarding the detailed structure of human dendritic spines. Technically, while electron microscopy can be used to accurately measure the dendritic spine structure, it is time-consuming and difficult, which makes it challenging to obtain large numbers of measurements. For example, the largest electron microscopic studies include at most 150 complete reconstructed dendritic spines (Arellano, Espinosa et al. 2007). Light microscopic techniques, although limited by the lower level of resolution, therefore remain the method of choice to obtain large-scale spatial information regarding the number and distribution of dendritic spines along the dendrites. At the same time, light microscopic studies normally estimate dendritic spine volumes from measurement of the spine head volumes, whereas spine necks are usually not included, due to the lack of software tools to reconstruct these structures accurately. Moreover, it is difficult to discriminate the border between the head and the neck in many cases. Because of these issues, there is a lack of studies that describe, in large numbers, the complete 3D structure of dendritic spines. To circumvent this problem, in the present study, we reconstructed the morphology of dendritic spines in 3Ds using a commercially available module software (Imaris surface) not specifically designed for spine reconstruction, but which allowed us to create our own protocol to precisely represent the spine morphology. In particular, we analyzed dendritic spines in the human cerebral cortex, which, as far as we are aware, have never been examined in 3D. Specifically, we manually analyzed over 8900 individual spines that were reconstructed along the length of the main apical and basal dendrites of layer III pyramidal neurons in the cingulate

cortex of 2 human males aged 40 and 85 years old, using intracellular injections of Lucifer Yellow (LY) in fixed cortical tissue. We find selective changes in dendritic and spine parameters with aging and a variety of morphological correlations between spine and dendritic morphologies. Also, a theoretical distribution is found for both volumes and lengths populations of dendritic spines.

Materials and Methods

Tissue Preparation

Samples obtained from 2 human males (aged 40 and 85) were used in this study. This tissue (kindly supplied by Dr I. Ferrer, Instituto de Neuropatología Servicio de Anatomía Patológica, IDIBELL-Hospital Universitario de Bellvitge, Barcelona, Spain) was obtained at autopsy (2–3 h post-mortem). These cases were used as controls in a previous study unrelated to the present investigation that was dealing with Alzheimer's disease (Blazquez-Llorca et al. 2010). The cause of death was traffic accident (case C40) and pneumonia plus interstitial pneumonitis (aged case, C85). Their brains were immediately immersed in cold 4% paraformaldehyde in 0.1 M phosphate buffer, pH 7.4 (PB) and sectioned into 1.5-cm-thick coronal slices. Small blocks of the cortex (ca. $15 \times 10 \times 10$ mm) were then transferred to a second solution of 4% paraformaldehyde in PB for 24 h at 4°C. In the present study, the tissue used was from the anterior cingular gyri (Brodmann's area 24; Garey 1994). Following neuropathological examination, C85 case showed abundant neurofibrillary pathology with the absence or scarcity of Abeta amyloid plaques in the hippocampal formation and adjacent cortex (parahippocampal cortex), but no neurofibrillar or amyloid pathology was found in areas 17, 18/19, or in temporal (areas 20 and 22), frontal (areas 8 and 10) or cingular (area 24) cortices. The C40 case had a Braak score of zero (Braak and Braak 1991; Mirra et al. 1991) for both pathologies.

Intracellular Injections

Coronal sections (250 μm) were obtained with a Vibratome and labeled with 4,6 diamino-2-phenylindole (DAPI; Sigma, St Louis, MO, United States of America) to identify cell bodies. Pyramidal cells were then individually injected with LY (8% in 0.1 M Tris buffer, pH 7.4), in cytoarchitectonically identified layer III of the anterior cingular gyrus. LY was applied to each injected cell by continuous current until the distal tips of each cell fluoresced brightly, indicating that the dendrites were completely filled and ensuring that the fluorescence did not diminish at a distance from the soma (for a detailed methodology of the cell injections, see Elston and Rosa 1997; Elston et al. 2001; Ballesteros-Yáñez et al. 2010).

Immunocytochemistry

Following the intracellular injection of pyramidal neurons (Fig. 1*A*), sections were immunostained for LY using rabbit antisera against LY (1:400 000; generated at the Cajal Institute) diluted in stock solution (2% bovine serum albumin, 1% Triton X-100, and 5% sucrose in PB). The sections were then incubated in biotinylated donkey anti-rabbit IgG (1:100; Amersham, Buckinghamshire, United Kingdom) and Alexa fluor 488 streptavidin-conjugated (1:1000; Molecular Probes, Eugene, OR, United States of America). Finally, sections were mounted in 50% glycerol in PB.

Imaging and Quantitative Analysis

Sections were imaged with a Leica TCS 4D confocal scanning laser attached to a Leitz DMIRB fluorescence microscope. Fluorescent

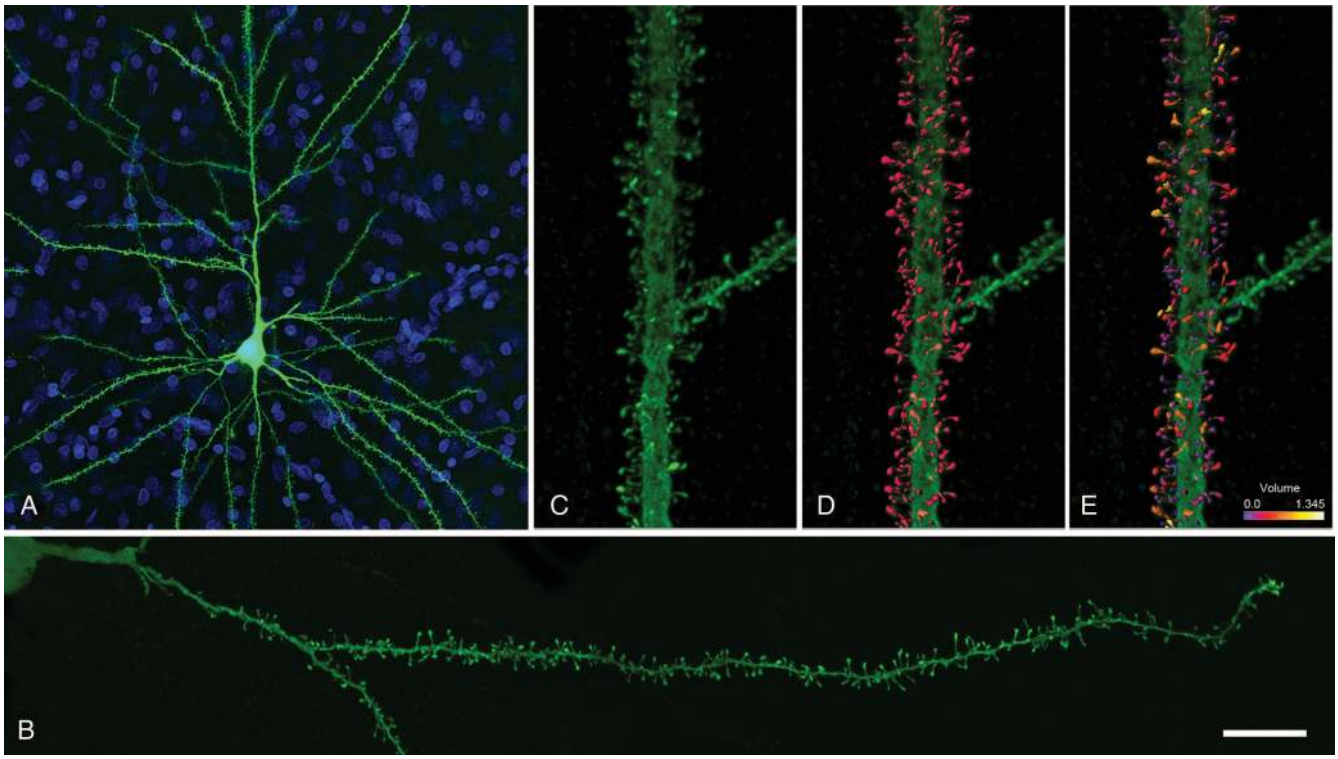

Figure 1. (*A*) Confocal microscopy image of an intracellular injected layer III pyramidal neuron of the human cingulate cortex. DAPI staining in blue. (*B*) High magnification image showing a horizontally projecting basal dendrite, to illustrate the extent of the labeling. Notice the virtual lack of dendritic spines in the proximal dendritic segment. (*C*) High magnification image of an apical dendritic segment acquired at 100 μm distance from the soma. (*D*) Three-dimensional reconstruction of the complete morphology of each dendritic spine shown in (*C*). (*E*) Estimation of the spine volume values shown in (*D*) by color codes (blue-white: 0.0–1.345 μm^3). Scale bar (in *B*): 40 μm in *A*; 13 μm in *B*; and 7 μm in *C*–*E*.

labeling profiles were imaged, using an excitation wavelength of 491 nm to visualize Alexa fluor 488. Horizontally projecting basal dendrites were randomly selected, each one originated from a different pyramidal neuron (10 per case). Consecutive stacks of images (3 ± 0.6 stacks per dendrite; 52 ± 17 images; z-step of 0.28 μm) were acquired at high magnification (×63 glycerol) to capture the full dendritic depth, length, and width of basal dendrites (30 stacks per case; Fig. 1*B*). The main apical dendrite was also scanned, at the same magnification, at a distance of 100 μm from the soma, since dendrites were virtually devoid of spines for the first 80–90 μm, up to 200 μm from the soma (8 dendrites per case; Fig. 1*C*). For each stack of images, confocal parameters were set so that fluorescence signal was as bright as possible while ensuring that there were no pixels saturated within the spines.

Spine structure was analyzed using Imaris 6.4.0 (Bitplane AG, Zurich, Switzerland). Since there are no clear limits between the head and the neck of a spine (Arellano, Benavides-Piccione et al., 2007), no such distinction was applied. Instead, we reconstructed the complete morphology of each dendritic spine in 3D (Fig. 1*D–E*). All dendritic spines were included and considered equally in the analysis. Correction factors used in other studies when quantifying dendritic spines with the Golgi method (Feldman and Peters 1979) were not used in the present study as the fluorescent labeling and the high-power reconstruction allowed the visualization of dendritic spines that protrude from the underside of dendrites. However, confocal stacks of images intrinsically result in a *z*-dimension distension; thus, a correction factor of 0.84 was applied to that dimension. This factor was calculated using a 4.2 μm Tetraspeck Fluorescent microsphere (Molecular Probes) under the same parameters used for the acquisition of dendritic stacks.

Dendritic spine density was determined by counting the number of dendritic spines per 10 μm of dendritic length, starting at the soma and continuing to the distal tips of basal dendrites. For apical dendrites, the 100 μm long segment was also analyzed every 10 μm of dendritic length. *Dendritic diameter* values were calculated per dendritic order in basal dendrites by measuring the diameter, in the *x–y* dimension of the stack, at the beginning and the end of the dendrite and before and after each dendritic node. Also, dendritic diameter was calculated every 10 μm along the length of the basal and apical dendrites. *Dendritic shaft volume* was additionally calculated for each dendrite, by selecting a particular threshold that represented a solid surface that matched the contour of the dendritic shaft (Fig. 2*A*,*B*). The *total volume of the dendrite* represents the sum of dendritic shaft volume and all dendritic spine volumes of the corresponding dendrite (*total dendritic spine volume*; see below for details of dendritic spine volume reconstruction).

Dendritic Spine Volume

To capture the whole range of dendritic spine volumes, 7–10 different intensity threshold surfaces were first created for each stack of images. Then, for each individual dendritic spine, a particular threshold was selected to constitute a solid surface that exactly matched the contour of each dendritic spine (Fig. 2*C*,*D*). However, sometimes it was necessary to use several surfaces of different intensity thresholds to capture the complete morphology of a dendritic spine.

Dendritic Spine Length

Dendritic spine length was manually marked in each individual dendritic spine from its point of insertion in the dendritic shaft to the distal tip of the spine, while rotating the image in 3Ds (Fig. 2*E*).

Dendritic Length

Dendritic length is a measure of the total length of each basal or apical dendrite and the *Number of dendritic spines* refers to all dendritic spines contained within the total length of each dendrite.

Statistics

All statistical analyses were performed using R and GraphPad Prism version 5.00 for Windows (GraphPad Software, San Diego, CA, United States of America). When morphological parameters were presented as mean values per dendrite and frequency distributions, the Kruskal–Wallis and Kolmogorov–Smirnov tests were used, respectively, to compare between the groups. The fit of the parametric distributions of morphological parameters was performed using the R package fitdistrplus. The fitting method used was the maximum-likelihood estimation. In this case, the Kolmogorov–Smirnov test was performed with a significance level of 0.05. Measurements reported as a function of the distance from the soma and branch order per dendrite were analyzed using 2-way ANOVA and the Bonferroni post-tests. Correlation analysis between the parameters quantified was performed using the Spearman analysis. Significant correlations were classified as weak [Spearman's rho (r) value lower than 0.40], moderate ($0.4 < r < 0.7$), and strong ($r > 0.7$). Differences were considered to be significant when $P < 0.05$. Measurements are reported as mean ± SEM, unless otherwise indicated.

Results

Analysis of Spine Densities

Over 8900 individual spines were completely 3-dimensionally reconstructed along 6.35 mm of dendritic length of main apical ($n = 16$) and basal dendrites ($n = 20$) of layer III pyramidal neurons in the cingulate cortex (area 24) of individuals C40 and C85. Figure 3 shows examples of apical and basal z-projection stacks of dendrites (76 stacks) in both cases. For each stack, several morphological parameters that included features of the dendritic shafts and spines were measured as described above.

First, we measured the spine density. Apical dendrites showed a significantly higher mean density than basal dendrites in both cases (Fig. 4*A*; see Supplementary Table S1). Furthermore, significant differences were found between all groups when frequency distributions were calculated (Fig. 4*B*; see Supplementary Table S2). Specifically, C85 basal dendrites presented the lowest density, followed by C40 basal dendrites and then C85 apical dendrites. C40 apical dendrites showed the highest density. We then analyzed the distribution of dendritic spines along the entire length of dendrites as a function of the distance from the soma to the distal tips of dendrites. We found that the basal dendritic spine density, at approximately 70–130 μm from the soma, was significantly lower in individual C85 than in individual C40 (Fig. 4*C*; see Supplementary Table S3). In particular, C40 dendritic spine density increased to a maximum of 1.870 spines/μm at 110 μm and then values slightly decreased along the remaining length of the basal dendrite. However, in basal dendrites of individual C85, the density increased to 1.2–1.3 spines/μm at approximately 90 μm from the soma and then the values remained similar along the remaining length of the dendrite (Fig. 4*C*). Regarding apical dendrites (Fig. 4*D*), individual C40 displayed significantly higher values than any other group along the length of the dendritic segment (Fig. 4*D*; see Supplementary Table S4). More specifically, values slightly increased to a maximum of 4.375 spines/μm (at 160 μm) in individual C40 and 2.250 spines/μm (also at 160 μm) in individual C85.

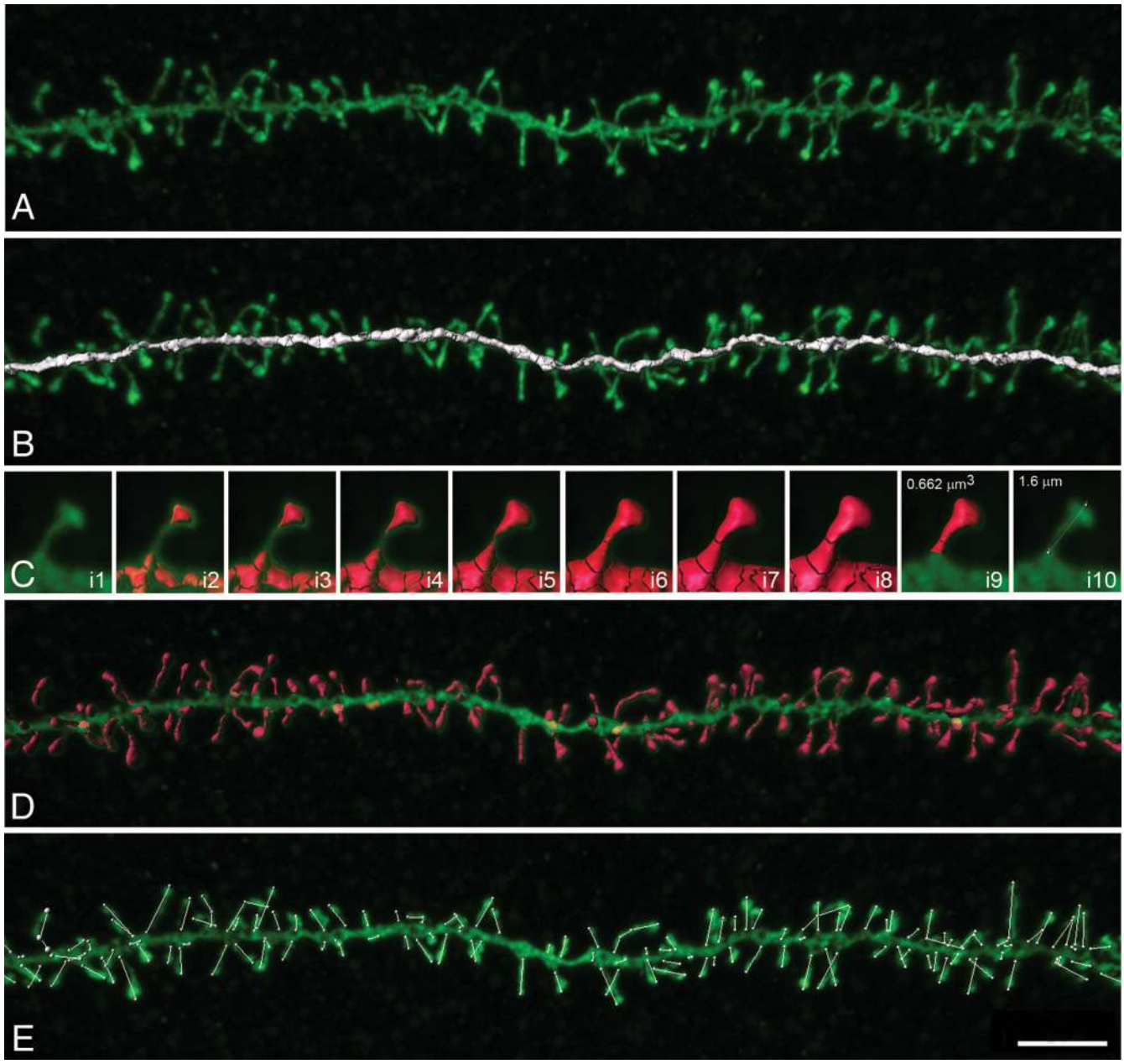

Figure 2. Dendritic shaft and dendritic spine reconstruction. (*A*) Confocal microscopy image showing a labeled basal dendritic segment. (*B*) For each dendrite, dendritic shaft volume (white) was 3D reconstructed by selecting a particular threshold that represented a solid surface that matched the contour of the dendritic shaft along the length of the dendrite. (*C*) To 3-dimensionally reconstruct the complete morphology of each dendritic spine, 7–10 different intensity thresholds were created (i1–8) and then, a particular threshold was selected to constitute a solid surface that exactly matched the contour of that dendritic spine (i9). (*D*) The sequence described in (*C*) was repeated for each individual dendritic spine to reconstruct each dendritic spine volume along the length of the dendrite. The combination of dendritic shaft volume and all dendritic spine volumes represents the total volume of the dendrite. (*E*) For each individual dendritic spine, its length was manually marked from its point of insertion in the dendritic shaft to the distal tip of the dendritic spine, while rotating the image in 3 dimensions (see i10 in *C*). Scale bar (in *E*): 6 μm in *A*, *B*, *D*, and *E* and 2.3 μm in *C*.

Analysis of Dendritic Diameter and Dendritic Volume

The mean values showed apical dendrites to have significantly greater diameters than basal dendrites (Fig. 4*E*; see Supplementary Table S1). The study of the cumulative frequency distribution revealed that apical, but not basal, curves were significantly different (Fig. 4*F*; see Supplementary Table S2). Dendritic diameters were then calculated as a function of the distance from the soma. As shown in Figure 4*G* and Supplementary Table S3, no significant differences were found between the basal dendrites of individuals C40 and C85. Additionally, basal dendritic diameters were analyzed per dendritic order (see Supplementary Fig. S1*A*). Again, no significant differences were found between individuals. Furthermore, the curves showed that values decreased as dendritic order increased, whereas when dendrites were analyzed as a function of the distance from the soma (Fig. 4*G*), the diameters decreased from the beginning of the dendrite to approximately 60 μm, with values then remaining similar

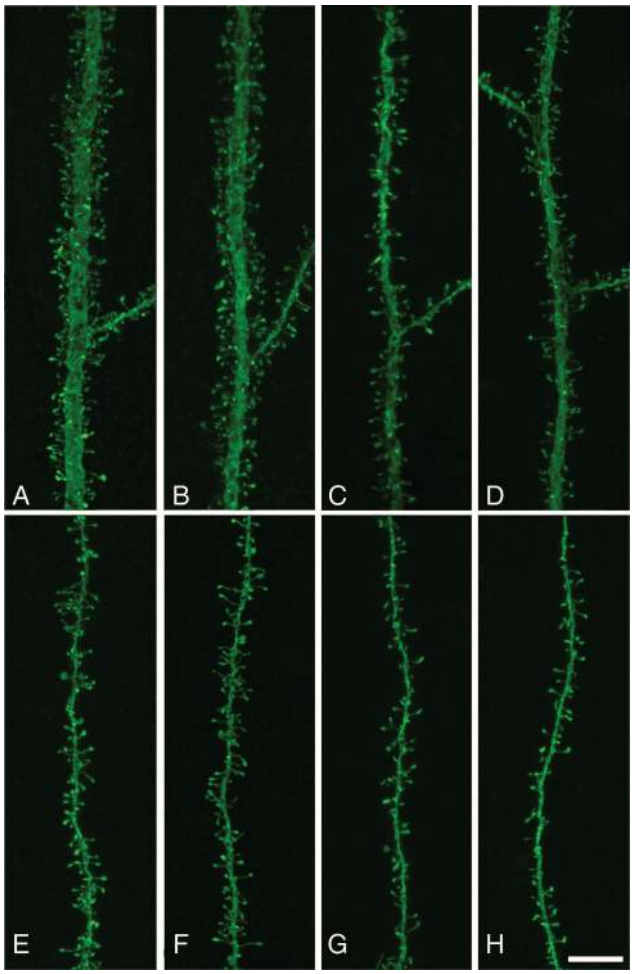

Figure 3. Examples of apical and basal dendritic segments. Confocal microscope images showing labeled apical (*A–D*) and basal (*E–H*) dendrites from case C40 (*A*, *B*, *E*, and *F*) and C85 (*C*, *D*, *G*, and *H*). Scale bar (in *H*): 6 μm in *A–H*.

along the length of dendrites and between both groups. Thus, it can be inferred that the position of bifurcations had to be located along the first approximately 60 μm. In fact, the estimation of the position of nodes showed that they were typically positioned between 11 ± 5 and 43 ± 11 μm and between 10 ± 4 and 38 ± 13 μm (mean ± SD; range 5–60 μm) for basal dendrites in individuals C40 and C85, respectively. Regarding the dendritic diameter of apical dendrites (Fig. 4*H*), C85 presented significantly thinner dendrites than C40 (see Supplementary Table S4). Additionally, apical dendrites of both individuals were statistically thicker than basal dendrites along the dendritic length). Regarding their distribution, the values remained relatively similar along the length of the dendritic segment.

Additionally, the dendritic shaft volume and the total volume of the dendrite were also calculated for each dendrite (see below for details of dendritic spine volume reconstruction). As shown in Table 1 and Supplementary Figure S1*B*, the estimated percentage of dendritic volume occupied by spines was 27% and 20% for C40 and C85, respectively, in apical dendrites and 33% and 27% for C40 and C85, respectively, in basal dendrites. Thus, there is a higher percentage of spines in C40 compared with C85, in both regions. However, there is a similar difference (6–7%) of higher dendritic volume occupied by dendritic spines in basal compared with apical dendrites, in both individuals.

Analysis of Dendritic Spine Volumes

We then reconstructed the complete morphology of each dendritic spine and measured their volumes (Fig. 2). The mean values (mean ± SEM; Fig. 5*A*) showed no significant differences between any of the groups (see Supplementary Table S1 for statistical comparisons). However, the study of their distributions (Fig. 5*B*,*C*; see Supplementary Table S2) revealed that basal dendrites from case C40 show the highest probability of having small dendritic spine volumes than any other group. Similarly, basal dendrites from case C85 show the highest probability of having large dendritic spine volumes compared with any other group. Indeed, significant differences were found between basal dendrites from cases C40 and C85. Additionally, significant differences were found between apical and basal dendrites in individual C40, but not in individual C85, which presented similar spine volumes.

To determine any possible underlying distributions of the volume data, the Cullen and Frey graph (skewness–kurtosis plot) was used. This graph revealed that spine volumes could be distributed as a gamma function (Fig. 5*D*). The maximum-likelihood estimates of the gamma distribution parameters were then computed for volume data (Fig. 5*E*). Estimated parameters along with the Kolmogorov–Smirnov goodness-of-fit statistic (KS test) can be found in Table 2. The KS tests determine that the empirical and the estimated distributions do not differ significantly. To further assess these results, the distributions, cumulative distribution functions (CDFs), QQ-plot, and PP-plot comparing the empirical (observed) distribution and the estimated gamma distribution were computed (see Supplementary Figs S2 and S3). The estimated gamma parameters (shape and rate) were smaller for dendritic spine basal volumes of individual C85 in comparison with the dendritic spine volumes of individual C40. Similarly, the same behavior was found in apical dendrites.

In addition, dendritic spine volumes were analyzed as a function of the distance from the soma, starting at the soma and continuing to the distal tips of basal dendrites (Fig. 6*A*) and along the 100–200 μm segment for apical dendrites (Fig. 6*B*). The results showed that basal dendrites of individual C85 displayed the highest values when compared with individual C40, although they did not reach statistical significance (see Supplementary Tables S3 and S4 for statistical comparisons). As shown in Figure 6*A*, the volume values of dendritic spines located along the first approximately 60 μm of the dendritic length of basal dendrites were relatively low and then increased to values that remained relatively similar along the rest of the dendritic segment. Regarding apical dendrites (Fig. 6*B*), volume values remained relatively similar along the apical dendritic segment (100–200 μm) in both C40 and C85 individuals. These values were similar to those observed in the basal dendrites at the same distance from the soma.

Analysis of Dendritic Spine Length

Apical dendrites from individual C40 had longer dendritic spines than those in basal dendrites, but not in individual C85 (Fig. 7*A*; see Supplementary Table S1). The detailed study of

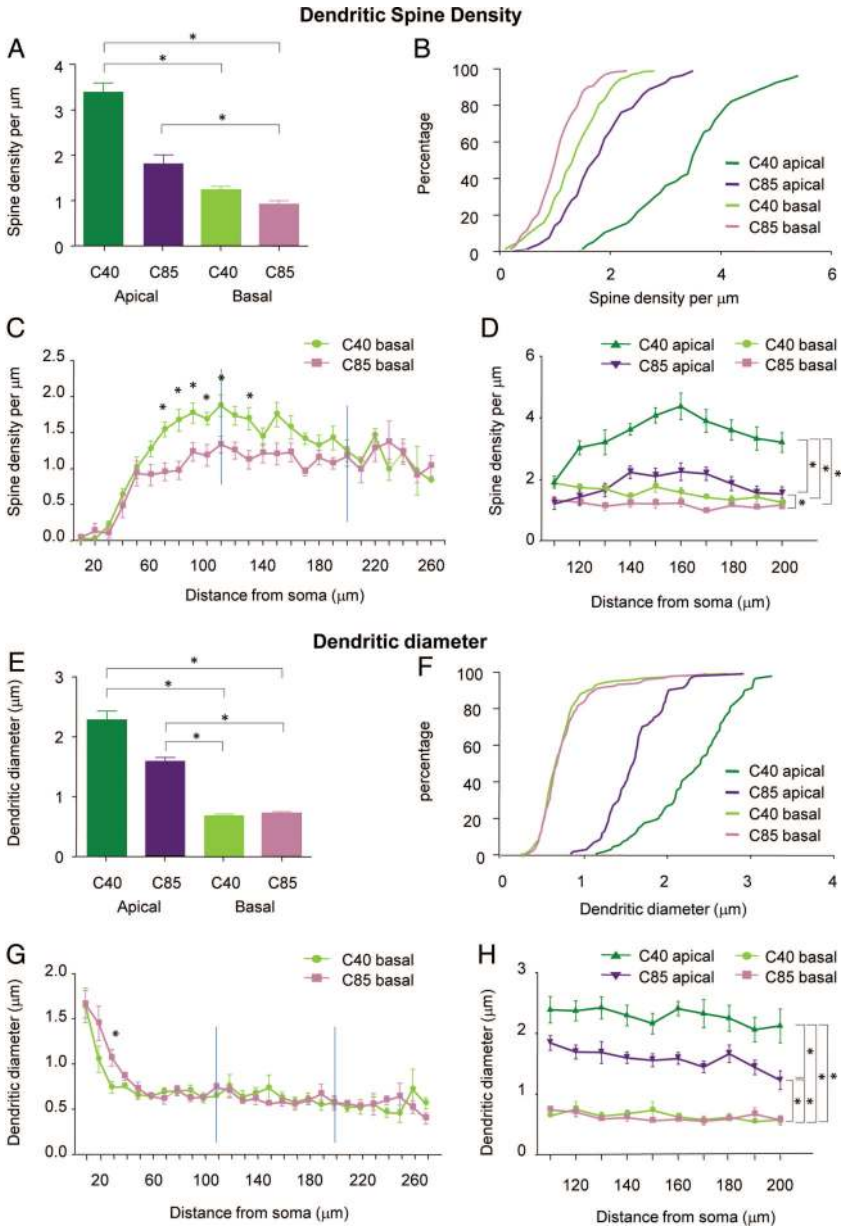

Figure 4. Dendritic spine density and dendritic diameter measurements in apical and basal dendrites. (*A–D*) Graphs showing the mean dendritic spine density (*A*), cumulative frequency distributions (*B*), and distribution of dendritic spine density as a function of the distance from the soma (*C* and *D*) in individuals C40 and C85. (*E–H*) Graphs showing the mean dendritic diameter (*E*), cumulative frequency distributions (*F*), and distribution of dendritic diameter as a function of the distance from the soma (*G* and *H*) in individuals C40 and C85. Blue lines in (*C*) and (*G*) correspond to the 100–200 µm segment of basal dendrites shown in the corresponding panels (*D*) and (*H*). Asterisks indicates the presence of significant differences. See Supplementary Tables S1–S4 for details of statistical comparisons.

these distributions of values (Fig. 7*B*,*C*) revealed that basal dendrites from case C40 showed the highest probability of having short dendritic spines compared with any other group, whereas apical dendrites from case C40 showed the highest probability of having long dendritic spines compared with any other group. Significant differences were found between all the groups (see Supplementary Table S2 for statistical comparisons).

As with dendritic spine volumes, their lengths were further analyzed to search for theoretical distributions and could also be estimated as gamma functions (Fig. 7*D*). Thus, the maximum-likelihood estimates of the gamma distribution parameters were computed for length data (Fig. 7*E*). Estimated parameters along with the Kolmogorov–Smirnov goodness-of-fit statistic can be found in Table 3. As can be seen in this

Table 1
Measurements (mean ± SD) of the total volume of the dendrite, dendritic shaft volume, and total dendritic spine volume[a] per dendrite, and percent of spine volume in individuals C40 and C85

	n	Total volume of the dendrite (µm^3)	Dendritic shaft volume (µm^3)	Total dendritic spine volume[a] (µm^3)	% of spine volume
All dendrites	36	268.28 ± 83.10	195.00 ± 64.29	73.28 ± 28.15	27.31
C40 apical	8	361.77 ± 64.37	264.07 ± 46.63	97.70 ± 27.85	27.01
C85 apical	8	248.49 ± 61.35	197.37 ± 53.20	51.11 ± 19.67	20.57
C40 basal	10	240.1 ± 64.21	160.48 ± 48.93	79.58 ± 20.2	33.15
C85 basal	10	237.55 ± 82.41	172.37 ± 64.38	65.18 ± 23.76	27.44

[a]Calculated as the sum of all spine volumes contained within the dendrite.

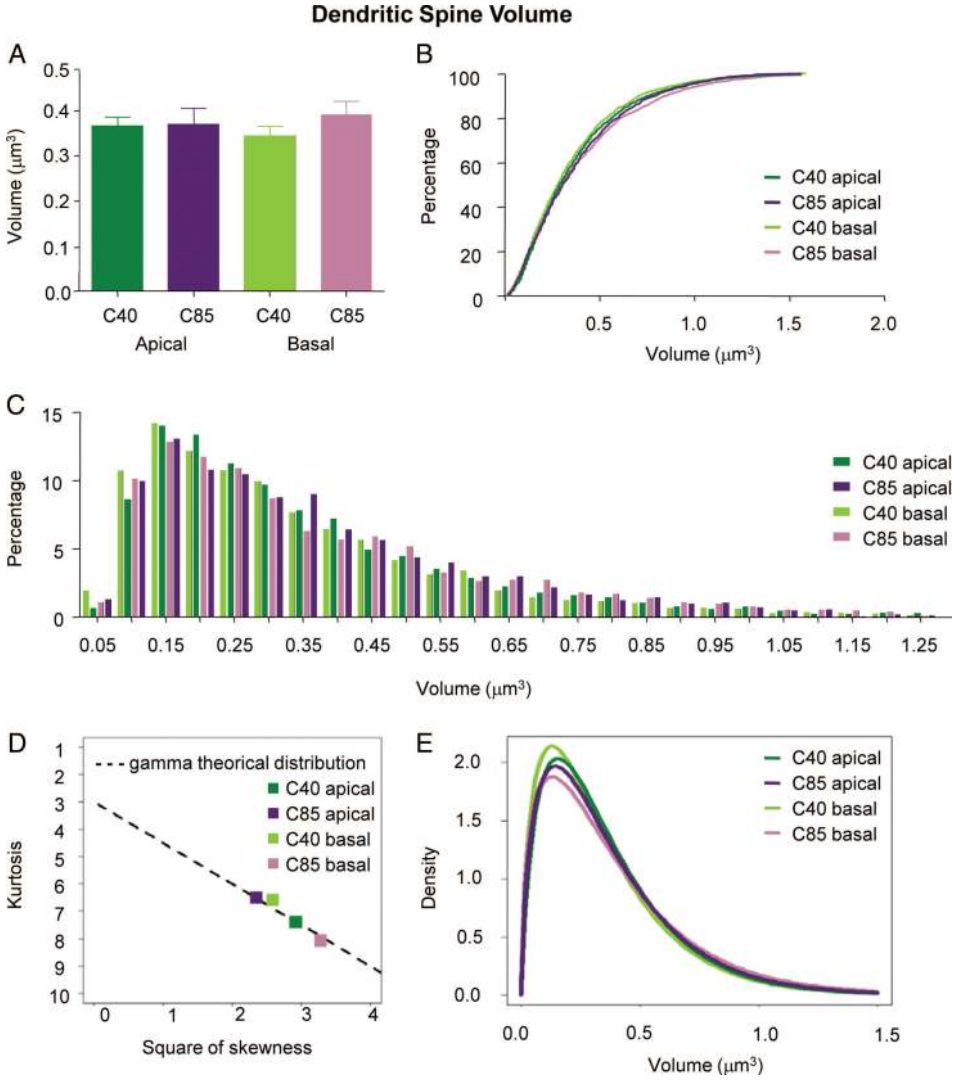

Figure 5. Dendritic spine volume analysis. (*A–C*) Graphs showing dendritic spine volume measurements represented as mean values per dendrite (*A*), cumulative distribution functions (*B*), and frequency distribution histograms (as percent) (*C*) in apical and basal dendrites of individuals C40 and C85. See Supplementary Tables S1 and S2 for statistical comparisons. (*D*) The Cullen and Frey graph (skewness–kurtosis plot) displaying the relationship between the square of skewness and the kurtosis of standard distributions for dendritic spine volumes. (*E*) Graph showing the density of the estimated gamma distributions for dendritic spine volumes from apical and basal dendrites of cases C40 and C85, with the parameters of shape and rate corresponding to Table 2.

table, the estimated gamma parameters for C40 basal and C85 basal are quite similar, and their intervals overlap. Supplementary Figs S4 and S5 show the Kolmogorov-Smirnov test, along with the distributions, CDFs, QQ-plot, and PP-plot comparing the empirical (observed) distribution and the estimated gamma distribution, which show that in all cases, spine lengths were distributed as a gamma function. When dendritic spine lengths were analyzed as a function of the distance from the soma (Fig. 6*C*,*D*), no significant differences were found between basal dendrites, whereas apical dendrites showed, in both cases C40 and C85, significantly higher values than those observed in the basal dendrites of individual C40 (see Supplementary Tables S3 and S4 for statistical comparisons). Finally, length values of dendritic spines located along the first approximately 60 μm of the dendritic length of basal dendrites were relatively low and then increased to values that that remained relatively similar along the rest of the dendritic segment. Regarding apical dendrites, values were similar along the length of the apical dendritic segment (100–200 μm) in both C40 and C85 individuals (Fig. 6*D*).

Table 2
Estimated gamma parameters and the Kolmogorov–Smirnov goodness-of-fit for dendritic spine volumes

	Estimated gamma parameters		Goodness-of-fit statistics
	Shape	Rate	Kolmogorov–Smirnov
C40 apical	1.75 ± 0.045	4.88 ± 0.145	0.036
C85 apical	1.64 ± 0.058	4.47 ± 0.186	0.028
C40 basal	1.61 ± 0.039	4.78 ± 0.137	0.022
C85 basal	1.51 ± 0.043	3.91 ± 0.133	0.036

Finally, the mean length of dendrites, the total dendritic length analyzed, the mean number of spines per dendrite,

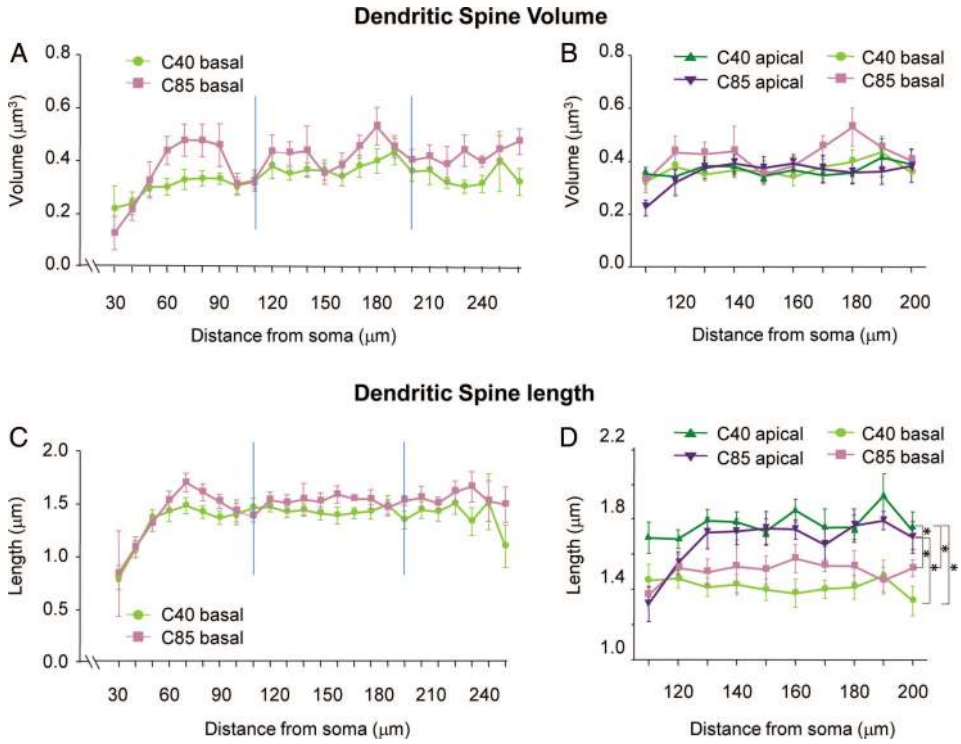

Figure 6. Dendritic spine volume and length measurements as a function of the distance from the soma. Graphs showing the distribution of values as a function of the distance from the soma for dendritic spine volumes (*A* and *B*) and lengths (*C* and *D*) in basal (*A* and *C*), and apical (*B* and *D*) dendrites in individuals C40 and C85. Blue lines in (*A*) and (*C*) correspond to the 100–200 μm segment of basal dendrites shown in the corresponding panels (*B*) and (*D*). Asterisks indicates the presence of significant differences. See Supplementary Tables S3 and S4 for details of statistical comparisons.

and the total number of spines found in each dendrite is shown in Table 4 (see also Supplementary Fig. S6 for further information).

Correlation Between Morphometric Parameters

We then examined whether there was a potential correlation, in apical and basal dendrites, between the different parameters analyzed in the present study. As shown in Figure 8, apical and basal compartments displayed independent relations. For example, the apical dendritic spine density displayed a strong correlation with dendritic diameter (Fig. 8*A*), whereas the basal dendritic spine density showed a strong negative correlation with dendritic spine volume (Fig. 8*B*). Additionally, basal spine volumes showed a moderate correlation with dendritic diameter (Fig. 8*D*). No other significant relation was found between these parameters. See also Supplementary Tables S5 and S6 for further apical and basal relations.

Discussion

The main findings in the present study are the following. First, we find a lower spine density and volume and shorter length of dendritic spines, and lower dendritic thickness in basal compared with apical dendrites. Second, except for the increase in densities, there is no systematic variation in spine morphologies with respect of distance from the soma. Third, we find positive correlations between apical spine densities and dendritic diameters, and negative correlations between basal spine densities and spine volumes. Fourth, a gamma theoretical distribution is followed by both volumes and lengths populations of dendritic spines. Finally, a major reduction in spine densities and apical dendritic thickness, as well as a decline in small and short spines in basal dendrites and long spines in apical dendrites, is observed with age.

Methodological Considerations

Our results in aging should be interpreted with caution since, although we analyzed thousands of individual 3-dimensionally reconstructed spines, they only come from 2 individuals. This limited number of cases was due to the difficulties in obtaining human tissue, especially with the optimal quality of fixation and preservation required for a detailed study of the complete morphology of the dendritic spines. A further point to be considered is that different cortical areas show remarkable differences in their structure and there is great interindividual variability (brain size, cortical thickness, number of cells, gender differences, etc.) (DeFelipe 2011). Therefore, the data obtained in the present study cannot be generalized to all cortical areas, genders and ages. Nevertheless, it is important to bear in mind that the human cerebral cortex is unique in many aspects, including genetic, molecular, structural, and physiological levels, and therefore, research on human brain is fundamental in spite of these limitations. The results obtained in the present study regarding intraindividual differences across dendritic compartments and theoretical distributions of dendritic spines are robust due to the large number of dendritic spines analyzed. Thus, the present study represents a further step toward the characterization of the human brain microorganization, but it would be necessary to confirm with a larger number of individuals

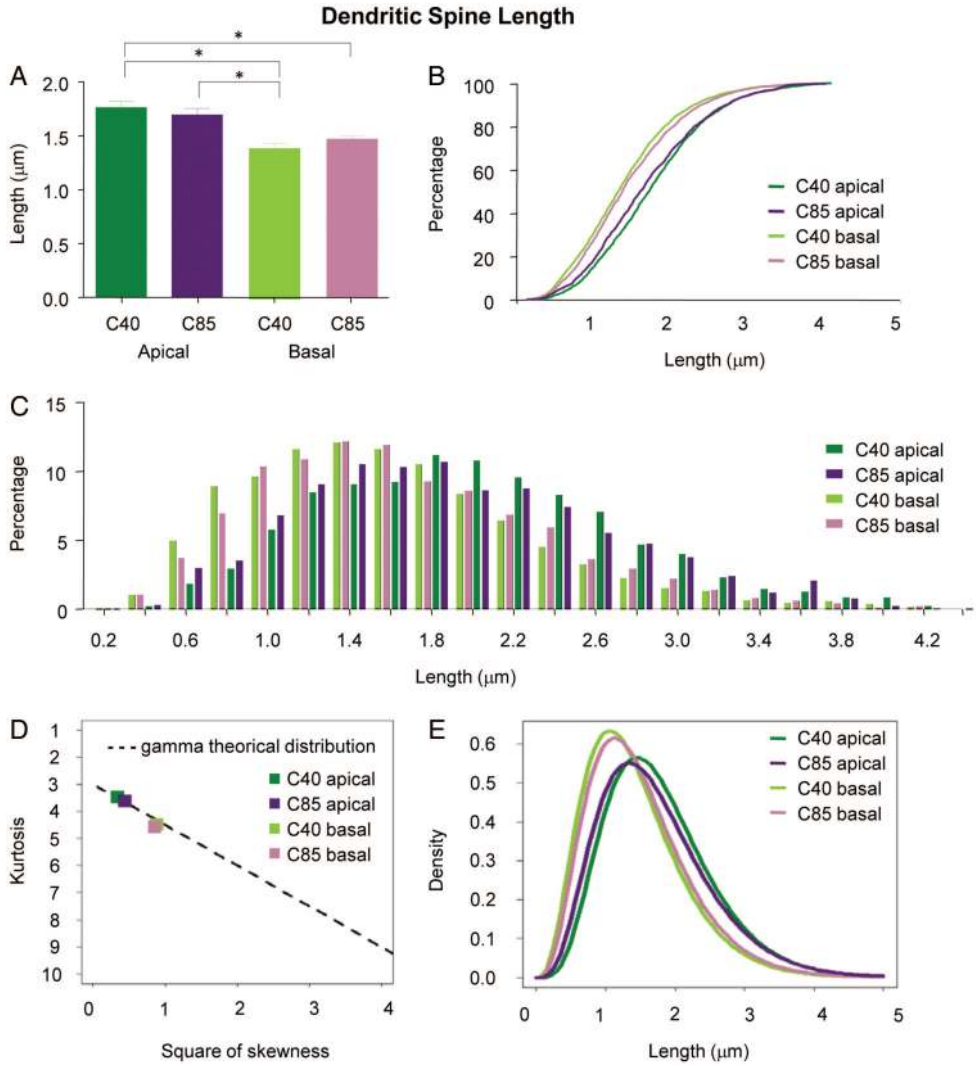

Figure 7. Dendritic spine length analysis. (*A–C*) Graphs showing dendritic spine length measurements represented as mean values (*A*), cumulative distribution functions (*B*), and frequency distribution histograms (as percent) (*C*) in apical and basal dendrites of individuals C40 and C85. See Supplementary Tables S1 and S2 for statistical comparisons. (*D*) The Cullen and Frey graph (skewness–kurtosis plot) displaying the relationship between the square of skewness and the kurtosis of standard distributions for dendritic spine lengths. (*E*) Graph showing the density of the estimated gamma distributions for dendritic spine lengths from apical and basal dendrites of cases C40 and C85, with the parameters of shape and rate corresponding to Table 3.

Table 3
Estimated gamma parameters and the Kolmogorov–Smirnov goodness-of-fit for dendritic spine lengths

	Estimated gamma parameters		Goodness-of-fit statistics
	Shape	Rate	Kolmogorov–Smirnov
C40 apical	5.38 ± 0.143	3.02 ± 0.084	0.032
C85 apical	4.59 ± 0.166	2.68 ± 0.103	0.027
C40 basal	4.00 ± 0.101	2.83 ± 0.076	0.021
C85 basal	4.18 ± 0.125	2.82 ± 0.090	0.015

Table 4
Measurements (mean ± SD) of the dendritic length and number of spines per dendrite of individuals C40 and C85

	n	Mean dendritic length (μm)	Total dendritic length (μm)	Mean number of spines	Total number of spines
All dendrites	36	176.4 ± 74.55	6349.66	247.9 ± 80.63	8926
C40 apical	8	100.6 ± 3.806	804.70	332.9 ± 68.20	2663
C85 apical	8	103.6 ± 1.706	829.08	177.8 ± 49.48	1422
C40 basal	10	242.1 ± 31.32	2420.69	285.8 ± 52.56	2858
C85 basal	10	229.5 ± 53.72	2294.59	198.3 ± 43.29	1983

and in additional cortical areas. What follows is a discussion of the main findings in this study.

Differences in Morphological Parameters in Different Dendritic Compartments

In general, apical dendrites had higher density of spines, larger diameters, and longer dendritic spines compared with basal dendrites, whereas differences in spine volumes were only present in the younger individual (see Fig. 9 for a schematic representation of the results).

Accordingly, the higher density of spines in apical dendrites would be associated with differences in the number of synaptic inputs. On another note, since dendritic diameters are associated with cable properties (Rall 1995), it is

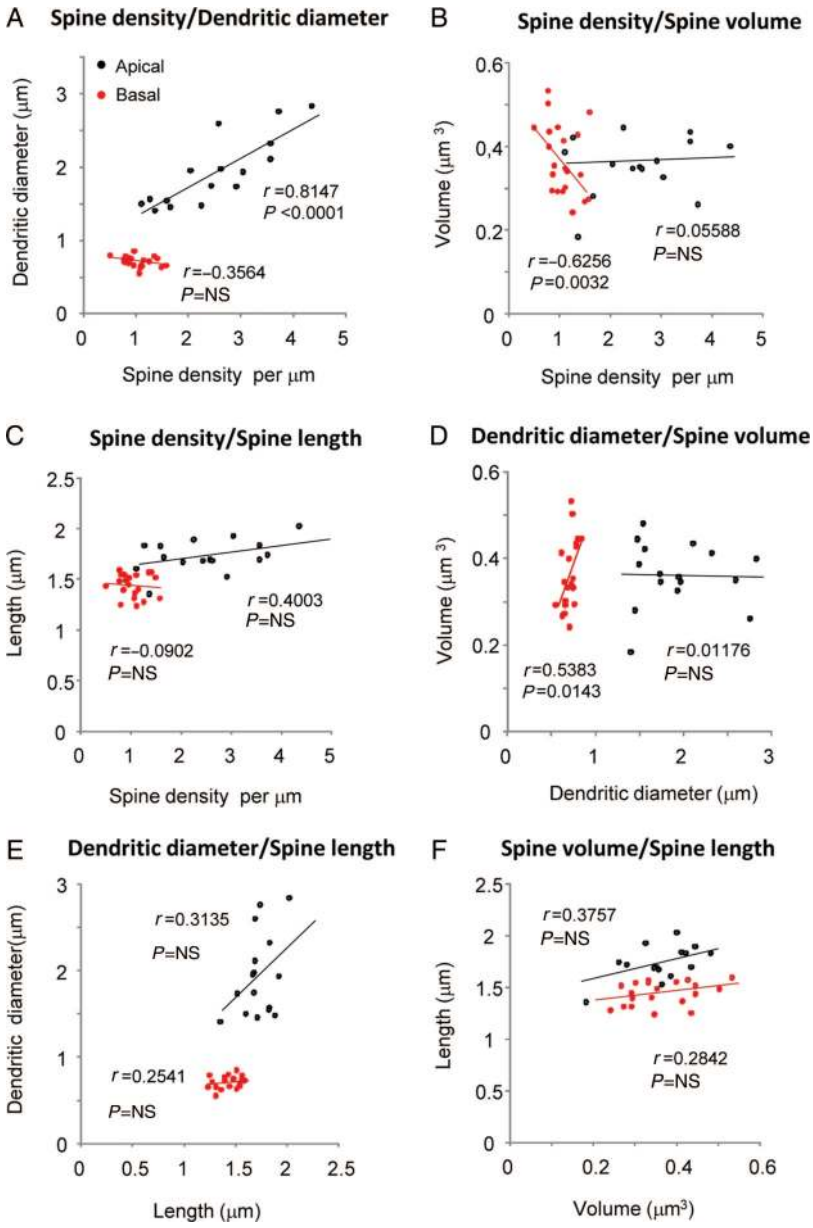

Figure 8. Correlation analyses in apical (black dots) and basal (red dots) regions between the various morphological parameters analyzed. Each point represents the values obtained in one dendrite of a different cell. Significant correlations were classified as weak [Spearman's rho (r) value lower than 0.40], moderate ($0.4 < r < 0.7$), and strong ($r > 0.7$). $n = 16$ dendrites for all apical comparisons and $n = 20$ dendrites for all basal comparisons. See also Supplementary Tables S5 and S6 for further apical and basal relations.

suggested that electric conductance of main apical dendrites is different from basal dendrites. The variability in spine length could be related to differences in biochemical compartmentalization (Yuste et al. 2000) in the different dendritic compartments of the neuron. Regarding spine volume, it is thought that small dendritic spines are preferential sites for long-term potentiation induction, whereas large spines might represent physical traces of long-term memory (Matsuzaki et al. 2004; Kasai et al. 2010). Thus, results suggest that the higher population of small spines present in basal dendrites could be related to a higher potential for plasticity in this dendritic compartment than in the apical dendrites. Altogether, these observations reveal that dendritic spines are structurally highly diverse between dendritic compartments, which in turn probably reflect differences in the processing of information.

As an additional interesting note, we found that there was a similar difference of 6–7% of higher dendritic volume occupied by dendritic spines in basal compared with apical dendrites, in both individuals. Thus, independent of the large differences found in absolute values between these individuals, dendritic spines seem to represent a fixed relative proportion in apical and basal dendrites of pyramidal neurons.

Distribution of Morphological Parameters as a Function of the Distance from the Soma

All parameters analyzed on basal dendrites showed increasing values for the first approximately 60 μm of dendritic length,

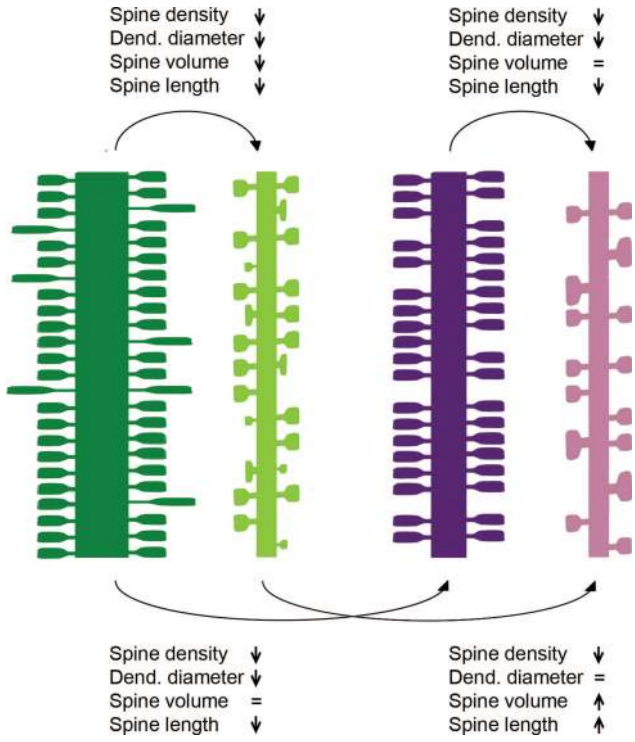

Figure 9. Schematic representation showing main statistical differences in morphological parameters found between apical (dark colors) and basal (light colors) dendritic compartments of individual C40 (green) and C85 (purple).

with the exception of the dendritic diameter, which decreased along the same distance (Fig. 4*G*). Then, values remained, in general, relatively similar along the remaining dendritic length, except for spine density, which reached a peak at 110 μm and then decreased. That is, there is a trend in the distribution of dendritic spine density along the length of the dendrite with respect to the soma. In particular, proximal dendritic segments are devoid of spines (typically for 10–15 μm) and they become increasingly more prevalent, reaching a peak at approximately one-third of the total length from the soma, and then gradually decreasing toward the tip of the dendrite. This distribution is in line with previous studies performed on a variety of species and cortical regions (Elston et al. 2001; Elston and DeFelipe 2002; Ballesteros-Yáñez et al. 2010).

In contrast, dendritic diameter, dendritic spine volume, and spine length are independent of their distance from the soma, from approximately 60 μm onwards. Previous studies in the neocortex of mice have also reported a lack of correlation between the spine size and the distance from the soma (Konur et al. 2003; Arellano, Benavides-Piccione et al. 2007). These observations suggest that there is no systematic compensation for the dendritic electrotonic filtering. These observations are at odds with previous studies that reported a larger dendritic spine size with increasing distance from the soma in several cortical regions and species, including the pyramidal neurons of the somatic sensory cortex of the cat and mouse primary visual cortex and of pyramidal neurons of the mouse and rat CA1 hippocampal region (Jones and Powell 1969; Megias et al. 2001; Konur et al. 2003). Thus, it is possible that this attribute is specific to the human cerebral cortex, but it may be simply that it depends on the cortical areas analyzed. Further studies would be necessary to resolve this question using the same methods.

Dendritic diameters of basal dendrites were additionally calculated per dendritic order, showing that the dendrite gets thinner as the dendritic order increases (see Supplementary Fig. S1). This indicates that, as predicted by the cable theory (Rall 1959), it is branch order and not the distance from the soma that determines diameter reduction. Regarding dendritic bifurcations, we observed Rall's $d^{3/2}$ constraint (Rall 1959) satisfied for the first 3-branch order. However, there was a deviation from this constraint in the decline in the dendritic diameter curve for the remaining branch orders, probably due to the lower frequency of higher branch orders. Additionally, we found all nodes to be located along the first approximately 60 μm from the soma, revealing that the distributions of dendritic spine volume and length values are, from the last dendritic bifurcation, independent of their distance from the soma. That is, as the dendrite is bifurcating, dendritic spine volume and spine length parameters show increasing values, whereas when the dendrite reaches a stable diameter for the remaining length, these parameters also stabilize. These results suggest a possible role of dendritic diameter as a regulatory factor in spine morphology.

Correlation Between Morphometric Parameters

First, we find that apical and basal compartments displayed different relations, which suggest that both compartments have independent rules for these parameters. This is in line with previous studies in the mice neocortex (Arellano, Benavides-Piccione et al. 2007) which also detected different relations for apical and basal compartments. In the present study, apical dendrites showed a correlation between dendritic spine density and dendritic diameter, suggesting a possible co-regulation of these variables in such a way that the greater the diameter of the dendrite, the greater the density of spines found in that dendrite. Instead, the basal spine density showed a strong negative correlation with dendritic spine volume, suggesting that the greater the density of spines, the smaller the size of spines. This is in line with previous studies in the mice neocortex (Konur et al. 2003) which detected a correlation between spine head diameter and interspine distance, whereby larger spines are spaced further away from each other than smaller spines. Also, a positive correlation was found between basal dendritic diameter and spine volume, indicating that thicker basal dendrites would have larger spines. However, differences in the thickness of basal dendrites were only found along the very first distances of the dendrite (Fig. 4*G*), whereas the majority of the dendritic length presents virtually identical values. Moreover, we fail to encounter significant correlations among the dendritic spine length and any other parameters, in both apical and basal dendrites. This indicates that the spine length is independently regulated from the spine volume, as if they were controlled by different biological mechanisms. The lack of correlation in spine volume and spine length parameters indicates that larger spines are not the longest. Thus, we confirm and extend previous findings in the mouse cerebral cortex (Benavides-Piccione et al. 2002) that these parameters are also independently regulated in the human neocortex.

In summary, thick apical dendrites tend to have a high density of spines but do not necessarily have larger/longer

spines. Basal dendrites seem to have a fixed dendritic diameter, and those with a greater density of spines have smaller sized spines.

Distribution of Dendritic Spine Volume and Lengths

The continuum of variability found in dendritic spine volumes reveals from the functional point of view a continuum of variability of axospinous synapses in both apical and basal human dendrites. Indeed, the large morphological diversity found, even for a small dendritic segment (Fig. 2), suggests an equally large variability of synaptic strengths and learning rules (Yuste 2010). Furthermore, we found that both dendritic spine volumes and lengths follow a theoretical distribution (gamma function). To our knowledge, there is no known biophysical explanation that accounts for why data may follow a gamma distribution, but it has been shown that other related phenomena, such as the interspike intervals, also follow a gamma distribution (Miura et al. 2007). Anyhow, it demonstrates that these components of cortical circuits are designed in accordance with the rules of mathematical functions. Thus, it will be possible to model functional maps of inputs on a given neuron, based on the hypothetical direct relation between the morphology of the dendritic spine and the synaptic current that each spine can generate. Further analyses in other cortical areas and species will help to determine whether the continuum of variability also found in their dendritic spines (Spacek and Hartmann 1983; Harris et al. 1992; Benavides-Piccione et al. 2002; Ballesteros-Yáñez et al. 2006; Arellano, Benavides-Piccione et al. 2007) follows the same theoretical function, suggesting a common organizational principle across species.

Selective Changes of Morphological Parameters in Aging in Apical and Basal Dendrites

We found that both apical and basal dendrites of individual C85 had significantly lower density of dendritic spines than those of individual C40 (Fig. 9), suggesting a general lower capability of neurons to integrate information in the aging brain. These observations are in agreement with previous studies on age-related changes performed in several cortical areas of primates, including humans (Rakic et al. 1994; Jacobs et al. 1997; Hof and Morrison 2004; Petanjek et al. 2008; Anderson et al. 2009; Kabaso et al. 2009; Dumitriu et al. 2010; Petanjek et al. 2011). We also found that apical dendrites of C85 were significantly thinner than apical dendrites of C40, whereas basal dendritic diameter remained similar in both individuals. Furthermore, the estimated percentage of dendritic volume represented by dendritic spines in C85 apical dendrites was lower (20%) than any other dendritic group (ca. 27–30%; Table 1). Thus, apical dendrites seem to be more sensitive to age-related changes than basal dendrites, in this regard. These results are in agreement with previous studies performed in monkeys which found that spine densities, dendrite diameters, lengths, and branching complexity were significantly reduced in apical dendrites of long projection neurons with aging (Kabaso et al. 2009).

Regarding dendritic spine volume, we find that basal dendrites from case C40 show the highest probability of having small dendritic spines, whereas C85 basal dendrites show the highest probability of having large dendritic spine volumes. Indeed, dendritic spines of C40 basal dendrites are significantly smaller than those in C85 basal dendrites. Thus, the main differences are found in basal dendrites, whereas apical dendrites remain more similar to each other, suggesting that small basal dendritic spine volumes may be selectively lost in aging. According to Matsuzaki et al. (2004) and Kasai et al. (2010), small dendritic spines are preferential sites for long-term potentiation induction, whereas large spines might represent physical traces of long-term memory. Thus, the higher percentage of small spines presented in basal dendrites of the 40-year-old case could be related to a higher potential for plasticity than in the aged case. These results are in line with previous studies performed in monkeys (Dumitriu et al. 2010), which showed that thin dendritic spine heads are lost with age.

Finally, we observed that basal dendrites from case C40 show the highest probability of having short dendritic spines, whereas the highest probability of having long dendritic spines occurs in C40 apical dendrites. Thus, apical and basal dendrites of C40 show greater differences between each other than C85 dendrites. Indeed, significant differences were found between all the groups. These results suggest that short spines of basal dendrites and long spines of apical dendrites may be lost with age. Since no previous studies in primates are available, we cannot conclude whether these results are a general characteristic of aged neurons.

In summary, taken together, the previous data and the present results show that since spine density is reduced in apical and basal compartments, a general lower capability to integrate information produced in all compartments of pyramidal neurons in the aging brain. Also, since dendritic diameter/shaft volume is specifically altered in apical dendrites, it is likely that the electrotonic conductance of pyramidal neurons is particularly altered in apical dendritic compartments. Additionally, long spines of apical dendrites and small and short spines of basal dendrites seem to be selectively lost, suggesting a reduction in preferential sites for long-term potentiation, and consequently, alterations in learning and memory in the aging brain.

Supplementary Material

Supplementary material can be found at: http://www.cercor.oxfordjournals.org/.

Funding

R.B.-P. was supported by the Ministerio de Economia y Competitividad (CSIC). J.D. was supported by grants from the following entities: Ministerio de Economia y Competitividad (grant SAF 2009-09394; and the Cajal Blue Brain Project, Spanish partner of the Blue Brain Project initiative from EPFL), CIBERNED (CB06/05/0066), and Fundación CIEN. R. Y. was supported by the HHMI and the National Eye Institute.

Notes

Conflict of Interest : None declared.

References

Anderson K, Bones B, Robinson B, Hass C, Lee H, Ford K, Roberts TA, Jacobs B. 2009. The morphology of supragranular pyramidal

neurons in the human insular cortex: a quantitative Golgi study. Cerebral Cortex. 19:2131–2144.
Araya R, Jiang J, Eisenthal KB, Yuste R. 2006. The spine neck filters membrane potentials. Proc Natl Acad Sci USA. 103:17961–17966.
Arellano JI, Benavides-Piccione R, DeFelipe J, Rafael Yuste R. 2007. Ultrastructure of dendritic spines: correlation between synaptic and spine morphologies. Front Neurosci. 1:131–143.
Arellano JI, Espinosa A, Fairén A, Yuste R, DeFelipe J. 2007. Non-synaptic dendritic spines in neocortex. Neuroscience. 145:464–469.
Ballesteros-Yáñez I, Benavides-Piccione R, Bourgeois JP, Changeux JP, DeFelipe J. 2010. Alterations of cortical pyramidal neurons in mice lacking high-affinity nicotinic receptors. Proc Natl Acad Sci USA. 107:11567–11572.
Ballesteros-Yáñez I, Benavides-Piccione R, Elston G, Yuste R, DeFelipe J. 2006. Density and morphology of dendritic spines in mouse neocortex. Neuroscience. 138:403–409.
Benavides-Piccione R, Ballesteros-Yáñez I, DeFelipe J, Yuste R. 2002. Cortical area and species differences in dendritic spine morphology. J Neurocytol. 31:337–346.
Blazquez-Llorca L, Garcia-Marín V, DeFelipe J. 2010. Pericellular innervation of neurons expressing abnormally hyperphosphorylated tau in the hippocampal formation of Alzheimer's disease patients. J Front Neuroanat. 4:20.
Bonhoeffer T, Yuste R. 2002. Spine motility. Phenomenology, mechanisms, and function. Neuron. 35:1019–1027.
Braak H, Braak E. 1991. Neuropathological stageing of Alzheimer-related changes. Acta Neuropathol. 82:239–259.
DeFelipe J. 2011. The evolution of the brain, the human nature of cortical circuits and intellectual creativity. Front Neuroanat. 5:29.
Dumitriu D, Hao J, Hara Y, Kaufmann J, Janssen WG, Lou W, Rapp PR, Morrison JH. 2010. Selective changes in thin spine density and morphology in monkey prefrontal cortex correlate with aging-related cognitive impairment. J Neurosci. 30:7507–7515.
Dunaevsky A, Tashiro A, Majewska A, Mason CA, Yuste R. 1999. Developmental regulation of spine motility in mammalian CNS. Proc Natl Acad Sci USA. 96:13438–13443.
Elston GN. 2007. Specializations in pyramidal cell structure during primate evolution. In: Kaas JH, Preuss TM, editors. Evolution of nervous systems. Vol. 4. Oxford: Academic. p 191–242.
Elston GN, Benavides-Piccione R, DeFelipe J. 2001. The pyramidal cell in cognition: A comparative study in human and monkey. Journal of Neuroscience. 21:RC163.
Elston GN, Benavides-Piccione R, Elston A, Manger PR, DeFelipe J. 2011. Pyramidal cells in prefrontal cortex of primates: marked differences in neuronal structure among species. Front Neuroanat. 5:2. doi: 10.3389/fnana.2011.00002.
Elston GN, DeFelipe J. 2002. Spine distribution in cortical pyramidal cells: a common organizational principle across species. Prog Brain Res. 136:109–133.
Elston GN, Rosa MG. 1997. The occipitoparietal pathway of the macaque monkey: comparison of pyramidal cell morphology in layer III of functionally related cortical visual areas. Cereb Cortex. 7:432–452.
Feldman ML, Peters A. 1979. A technique for estimating total spine numbers on Golgi impregnated dendrites. J Comp Neurol. 188:527–542.
Garey LJ. 1994. Brodmann's localisation in the cerebral cortex. London (UK): Smith-Gordon.
Harris KM, Jensen FE, Tsao B. 1992. Three-dimensional structure of dendritic spines and synapses in rat hippocampus (CA1) at postnatal day 15 and adult ages: implications for the maturation of synaptic physiology and long-term potentiation. J Neurosci. 12:2685–2705.
Harris KM, Stevens JK. 1989. Dendritic spines of CA1 pyramidal cells in the rat hippocampus: serial electron microscopy with reference to their biophysical characteristics. J Neurosci. 9:2982–2997.
Hof PR, Morrison JH. 2004. The aging brain: morphomolecular senescence of cortical circuits. Trends Neurosci. 27:607–613 (Review).
Jacobs B, Driscoll L, Schall M. 1997. Life-span dendritic and spine changes in areas 10 and 18 of human cortex: a quantitative Golgi study. J Comp Neurol. 386:661–680.
Jacobs B, Schall M, Prather M, Kapler L, Driscoll L, Baca S, Jacobs J, Ford K, Wainwright M, Treml M. 2001. Regional dendritic and spine variation in human cerebral cortex: a quantitative study. Cereb Cortex. 11:558–571.
Jacobs B, Scheibel AB. 2002. Regional dendritic variation in primate cortical pyramidal cells. In: Schüz A, Miller R, editors. Cortical areas: unity and diversity. London (UK): Taylor & Francis. p. 111–131.
Jones EG, Powell TPS. 1969. Morphological variation in the dendritic spines of the neocortex. J Cell Sci. 5:509–529.
Kabaso D, Coskren PJ, Henry BI, Hof PR, Wearne SL. 2009. The electrotonic structure of pyramidal neurons contributing to prefrontal cortical circuits in macaque monkeys is significantly altered in aging. Cereb Cortex. 19:2248–2268.
Kasai H, Fukuda M, Watanabe S, Hayashi-Takagi A, Noguchi J. 2010. Structural dynamics of dendritic spines in memory and cognition. Trends Neurosci. 33:121–129.
Konur S, Rabinowitz D, Fenstermaker V, Yuste R. 2003. Systematic regulation of spine head diameters and densities in pyramidal neurons from juvenile mice. J Neurobiol. 56:95–112.
Majewska A, Brown E, Ross J, Yuste R. 2000. Mechanisms of calcium decay kinetics in hippocampal spines: role of spine calcium pumps and calcium diffusion through the spine neck in biochemical compartmentalization. J Neurosci. 20:1722–1734.
Majewska A, Tashiro A, Yuste R. 2000. Regulation of spine calcium compartmentalization by rapid spine motility. J Neurosci. 20:8262–8268.
Matsuzaki M, Honkura N, Ellis-Davies GC, Kasai H. 2004. Structural basis of long-term potentiation in single dendritic spines. Nature 429:761–766.
Matus A. 2000. Actin-based plasticity in dendritic spines. Science 290:754–758.
Megias M, Emri Z, Freund TF, Gulyas AI. 2001. Total number and distribution of inhibitory and excitatory synapses on hippocampal CA1 pyramidal cells. Neuroscience 102:527–540.
Mirra SS, Heyman A, McKeel D, Sumi SM, Crain BJ, Brownlee LM, Vogel FS, Hughes JP, van Belle G, Berg L. 1991. The Consortium to Establish a Registry for Alzheimer's Disease (CERAD). Part II. Standardization of the neuropathologic assessment of Alzheimer's disease. Neurology. 41:479–486.
Miura K, Tsubo Y, Okada M, Fukai T. 2007. Balanced excitatory and inhibitory inputs to cortical neurons decouple firing irregularity from rate modulations. J Neurosci. 27:13802–13812.
Nusser Z, Lujan R, Laube G, Roberts J, Molnar E, Somogyi P. 1998. Cell type and pathway dependence of synaptic AMPA receptor number and variability in the hippocampus. Neuron. 21:545–559.
Petanjek Z, Judas M, Kostović I, Uylings HB. 2008. Lifespan alterations of basal dendritic trees of pyramidal neurons in the human prefrontal cortex: a layer-specific pattern. Cereb Cortex. 18:915–929.
Petanjek Z, Judaš M, Šimic G, Rasin MR, Uylings HB, Rakic P, Kostovic I. 2011. Extraordinary neoteny of synaptic spines in the human prefrontal cortex. Proc Natl Acad Sci USA. 108:13281–13286.
Rakic P, Bourgeois JP, Goldman-Rakic PS. 1994. Synaptic development of the cerebral cortex: implications for learning, memory, and mental illness. Prog Brain Res. 102:227–243 (Review).
Rall W. 1959. Branching dendritic trees and motoneuron membrane resistivity. Exp Neurol. 1:491–527.
Rall W. 1995. In: Segev I., Rinzel J., Shepherd G. editors. The theoretical foundation of dendritic function. Massachusetts: MIT Press.
Schikorski T, Stevens C. 1999. Quantitative fine-structural analysis of olfactory cortical synapses. Proc Natl Acad Sci USA. 96:4107–4112.
Schikorski T, Stevens CF. 2001. Morphological correlates of functionally defined synaptic vesicle populations. Nat Neurosci. 4:391–395.
Spacek J, Hartmann M. 1983. Three-dimensional analysis of dendritic spines. I. Quantitative observations related to dendritic spine and synaptic morphology in cerebral and cerebellar cortices. Anat Embryol. 167:289–310.
Yuste R. 2010. Dendritic spines. Cambridge (MA): MIT Press.
Yuste R, Majewska A, Holthoff K. 2000. From form to function: calcium compartmentalization in dendritic spines. Nat Neurosci. 3:653–659.